Engineering Solid Mechanics 10 (2022) 201-214

Contents lists available at GrowingScience

Engineering Solid Mechanics

homepage: www.GrowingScience.com/esm

Solar dome integration as technical new in water desalination: case study Morocco region Rabat-Kenitra

Saad Eddin Lachhab[a*], A. Bliya[a], E. Al Ibrahmi[a] and L. Dlimi[a]

[a]*Laboratory of Renewable Energies and Environment, Faculty of Sciences, IbnTofail University, BP. 133.14000-Kenitra, Morocco*

ARTICLE INFO

Article history:
Received 26 January 2022
Accepted 10 April 2022
Available online
11 April 2022

Keywords:
Solar dome
Water desalination
Concentration rate
Dew point temperature
Saturation pressure

ABSTRACT

This paper presents a study of the solar dome system that is considered as one of the most important economical solutions in the domain of drinking water production. For this, a mathematical model was built from equations describing the optical and thermal phenomenon involved in this process. The concentration of radiation and the heat flow were simulated in each 0.1m² of the dome using the metrological parameters of Morocco's region Rabat-Salé-Kenitra. The results can follow the evolution of the temperature of glass, salt water, point dew temperature, saturation pressure and evaporation rate as well as humidity reached in August month for the study zone. For this, a numerical implementation on Matlab and Ansys are compared with measurements for the same parameters shown in the domain study of single slope. The comparison results are more significant by the rise of the ray concentration rate reached to 99% if the inclination angle of the heliostat is divided into three intervals. The saturation pressure increases as long as with the rate of evaporation and the humidity that produces ordinary daily fresh water.

Nomenclatures

$Q_{c,w-g}$	: Convective heat transfer rate from water to glass cover (W/m²)
$Q_{e,w-g}$	: Evaporative heat transfer rate from water to glass cover (W/m²)
$Q_{c,g-a}$	: Conductive heat transfer rate from glass inner surface to outer surface cover (W/m²)
$Q_{r,g-a}$	: Heat transfer due to convection between glass and the air flow (W/m²)
$Q_{r,w-g}$	: Radiative heat transfer rate from water to glass cover (W/m²)
$h_{c,w-g}$	: Convective heat transfer coefficient from water to glass cover (W/m²K)
$h_{e,w-g}$	: Evaporative heat transfer coefficient from water to glass cover (W/m² K)
$h_{r,w-g}$	: Radiative heat transfer coefficient from water to glass cover (W/m² K)
$h_{c,g-a}$	: Convective heat transfer coefficient water to air (W/m² K)
$h_{r,g-a}$	: Convective heat transfer coefficient from air to glass (W/m² K)
$\dot{q}_{\lambda,solar}$	: Heat transfer (W)
$I_{\lambda,solar}$	: Solar intensity (W/m²)
T_a	: Ambient temperature (◦C)
T_{sky}	: Sky temperature (◦C)
T_{dp}	: Dew temperature :(◦C)
T_w	: Temperature of water (◦C)

* Corresponding author. Tel: +212637-030-707
E-mail addresses: saadeddinlachhab0@gmail.com (S. E. Lachhab)

doi: 10.5267/j.esm.2022.4.006

T_g : Temperature of glass surface (◦C)
P_w : Partial vapour pressure at water inner surface temperature (mbar)
P_g : Partial vapour pressure at glass inner surface temperature (mbar)
P_{ws} : Saturation pressure of $(H_2O)_g$(mbar)
P_{atm} : Atmospheric pressure, (mbar)
$G(t)$: Solar ray in basin (w/m²)
$M(H_2O)$: Molar mass of water (g/mol)
R : Dome radius (m)
H_i : stack height of helostats (m)
S_n : Area of heliostat (m²)
$d\Omega_{\text{helosta}}$: Solid angle heliostat
$d\Omega_{\text{dome}}$: Solid angle (sr)
dA : Area of mirror (m²)
s_d : Area of dome solar (m²)
$\frac{\vec{r}}{r^3}$: Field flux crossing the surfaces$_d$
$\vec{n}$: Unit vector giving the direction of the surface element;
Greek symbols
ϕ : Relative humidity
$d\lambda$: Radiative power
$\hat{n}$: Normal
$\vec{r}$: Position
β : Inclination angle
φ : Azimuth angle ψ
θ : Altitude angle
ε_{eff} : Effective emissivity between water surface and glass cover
σ : Stefan Boltzmann constant
ε_g : Effective remittances
$\alpha_g^{'}$: Transmissivite of the glass
$\alpha_w^{'}$: Transmissivite of the water

Abbreviation

PVGIS : Photovoltaic Geographical Information System
DNI : Direct Normal Irradiation

1. Introduction

Scarcity of water resources has become a big challenge in many countries around the world, especially in arid, semi-arid and coastal regions. Industrial development, economic prosperity and high population density, as well as successive years of drought and overexploitation of groundwater, are the main factors which have contributed negatively to the scarcity of this vital material. Many world health and environment organizations (Bekker et al. 2021) have warned in numerous conferences and reports that the water crisis will become a global health tragedy if urgent solutions to the problem are not sought. Despite the scientific and technical progress of the industries related to water production and the strategies followed to supply this substance, 3.1 billion people still suffer from a lack of water(Vega-Rodríguez et al. 2021) and depend on sources unsuitable for fresh water. On the African continent drinking waste water causes about 360,000 deaths (Nyiwul 2021). Many governments (Ouda et al. 2021) compete with each other to make the drinking water sufficient for their citizens by regulating and rationing water consumption to ensure that it reaches their residents in all regions, regardless of climatic conditions that affect them. Like the countries of sub-Saharan Africa and the Sahel, some African countries, such as South Africa, Tanzania and Morocco, have adopted water policies (Mwandila et al., 2021) which are mainly based on innovation and the integration of new solutions such as seawater desalination.

Desalination technologies play an important role in our daily life due to the increasing demand for clean water. In general, the technique of seawater desalination is known as the process of separating water molecules from the rest of other mineral substances (Lrhoul et al., 2021). This technique was known since ancient times and even by natural phenomena, when the temperature of the water increases, the water molecules evaporate under atmospheric pressure$P_{atm} = 1atm$, and after that they condense to become in the form of vapor carrying a large quantity of water transformed into pure and fresh water with the decrease in pressure or vapor temperature. This simple natural process has been used to suggest and develop many techniques(Chauhan et al., 2021) in this area. In this sense, more than 20 technologies (Shukla 2021) in the field of seawater treatment have been recognized, but they are divided into two main categories: the technique of evaporation-condensation (Khan et al., 2021) and the technique of reverse osmosis (Liu et al., 2021).

The use of the reverse osmosis method is one of the important methods that have been included in this list to work alongside seawater desalination techniques. The idea is mainly limited to applying high pressure to a certain amount of saline water inside a container separated by a membrane that contains thousands of holes whose diameter is equal to the diameter of the water molecule. Numerous studies have indicated several advantages and disadvantages of this technology, and most studies prove that reverse osmosis technology limits more than 98%(Chauhan et al., 2021) of non-invalid minerals. In addition, this technique does not use chemicals during the desalination process and the application can extend even for wastewater(Ali et al., 2021) . On the other hand, despite the importance of this technique and its dissemination in many countries, it remains a complicated and expensive method in terms of energy consumption (Patel et al., 2021). To produce each m^3 is needed 6 kwh electricity (Lin et al., 2021). Therefore, many countries resort to the cheapest and most efficient technologies, such as the use of thermal methods (Anand et al., 2021) to distil large quantities of water and in this area there are many techniques, the most famous is the low temperature multi-effect distillation technology (Khlaifat et al., 2020). However, these technologies face many difficulties in terms of maintenance of heat transfer tubes and high rates of rust, which limits their effectiveness. Especially, if the later technic used in some countries those have beaches with high concentration of salinity, such as the Dead Sea, which contains more than 34% of salinity. Therefore, it is necessary to think of solutions that can reduce the cost of desalination of seawater, increase its quality and reduce maintenance to improve the desalination capacity regardless of the salt concentration. The aim of this research is to highlight a new technique in the desalination of seawater with the aim of producing this vital material, especially for countries suffering from drought and poverty.

The solar dome technology (Figueroa et al., 2021) offers a promising opportunity in the field of water desalination, which provides solutions to most of the problems facing the various desalination technologies of this domain. The idea is based on the principle of evaporation and condensation by producing a quantity of vapor and confining it in a glass space for condensation and then transforming it into fresh water. The methodology is focused on the construction of a hemispherical glass dome surrounded by a set of heliostats on different radius Fig.1 (a). All heliostats (Lai et al., 2021) are fixed at heights defined according to the solid angle where the rays can be reflected Fig.1 (b). Inside the solar dome is a basin of depth 3m of and area$18 \times 18\ m^2$. A channel of radius R = 20 cm is installed around the inner side of the solar dome which collects the water drops formed on the sides of the hemispherical dome, Fig.1 (c). Each heliostat will be guided at the base of the inclination angle β, and in this regard a mathematical study will be detailed in order to compare the results depending on the amount of radiation produced and the rate of concentration at different angles. An optical and geometric discretization also carried out on 1000 part of 0.1m² area using a mesh was written in order to simulate the different thermal energies involved in the production of heat. The equations discretizing the temperatures, of both glass and dirty water, have been simplified and arranged in a 2 × 3 matrix in the form of a differential equation. The matrix will be solved using the Runge Kutta method of order 4 (ElHelw et al., 2020). The solution founded help to analyze the amount of evaporation as a function of temperature of both glass and dirty water and water pressure. To gather this data help us to calculate the saturation pressure and dew temperature which allows producing drops of water given the importance of humidity during the August month. Finally if we based on the point dew temperature and pressure, the quantity of water produced during this summer day will be estimated and simulated.

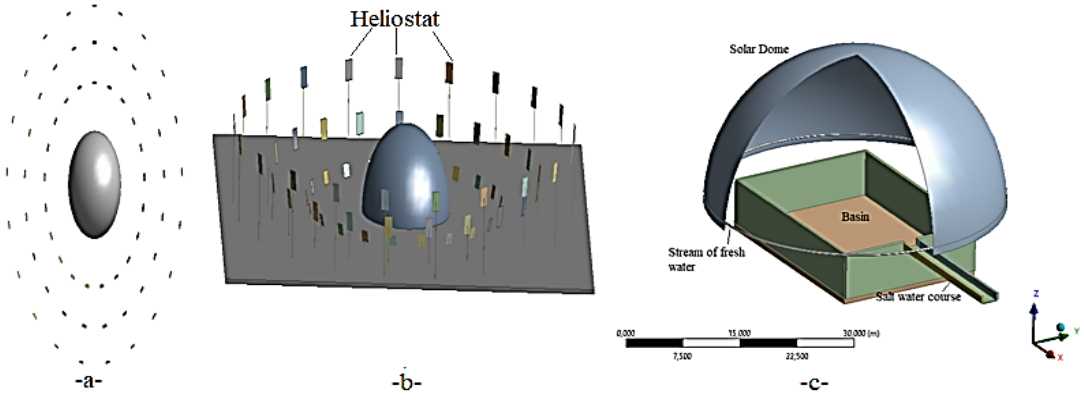

Fig.1. Central desalination of water by the technique of solar dome

1.1 Discretization of the mathematical model proposed for the solar desalination plant

Fig. 2 shows the schematic 2D diagram of the solar dome technique. The system consists mainly of four elements, the solar ray, the half-sphere-shaped dome, the seawater and the basin. The sun's rays emitted are divided into two main parts. The first part goes straight to the dome without being refracted or reflected. On the other hand due to the changing position of the sun during the day, the second part consists of installing mirrors in a position which helps to capture a large amount of the sun's rays and reflect them towards the dome during the day. The amount of radiation received on a hemispherical dome surface element dA_{rec}, is composed by the integration of the intensity of solar irradiation $I_{\lambda,solar}(\vec{r},\lambda,\hat{s})$(Bonanos et al., 2019). This intensity is characterized by the unitary direction $\hat{s}$ of each mirror and each position $\vec{r}$. On the other hand $\hat{s}$is linked to

the polar angle θ measured from the surface normal $\hat{n}$ and azimuth angle ψ (measured between an arbitrary axis on the surface).

$$\dot{q}_{\lambda,solar}(\vec{r}) = \int_{\lambda=0}^{\infty} \int_{A_{rec}} \int_{\Omega=0}^{2\pi} I_{\lambda,solar}(\vec{r},\lambda,\hat{s}) |\hat{n}.s| d\Omega\, dA d\lambda \tag{1}$$

1.2 Sphere concentration ray rate

Among the most important elements that allow us to know the efficiency of the system is the rate of concentration(Ashour et al., 2021) of sunlight. On the other hand, the concentration rate will be defined as the ratio of the area which receives the solar flux in a solid angle dΩ of the solar dome and the area of the 60 dimensional mirrors $s_n = 6\text{m} \times 3\text{m}$. An approximation has been established in a half-sphere of radius r, infinitesimal angular variations altitude dθ, azimuth dφ and we obtained Eq. (2).

$$\begin{cases} C = \dfrac{d\Omega_{\text{dome}}}{d\Omega_{\text{helosta}}} = \dfrac{\int_0^{\frac{\pi}{2}} sin\theta d\theta \int_0^{\pi} d\varphi}{\sum_{i=1}^{n=80} \cos\beta \times s_n} \\ d\Omega_{\text{dome}} = \iint_{s_d} \dfrac{\vec{r} \times \vec{n}}{r^3} d^2 s_d \end{cases} \tag{2}$$

s_d : Surface of the dome (m²)
$\frac{\vec{r}}{r^3}$: Field flux crossing the surface s_d
$\vec{n}$: Unit vector giving the direction of the surface element

A study on the radiation concentration rate was developed on software, Matlab, with the 60 heliostats distributed on a circular face with radius R1 = 35 m, R2 = 45 m, R3 = 55 m and height H1 = 1 m, H2 = 10 m and H3 = 15m. The heliostats are distributed around the axis $\overrightarrow{oz}$ at an angle $\varphi = 20°$ with an area of 6 m² for each mirror. The angle of inclination β, see Fig.2, will be oriented at angular intervals(Xiao et al., 2021) respecting the following conditions:

Circle 1: radius $R_1 = 35\ m$, height $H_1 = 1\ m$ and β_1 varies between 0° and 30°
Circle 2: radius $R_2 = 40\ m$, height $H_2 = 10m$, $\beta_2$varies between30° and 60°
Circle 3: radius $R_1 = 55\ m$, height $H_1 = 15\ m$, $\beta_3$varies between60° and 90°

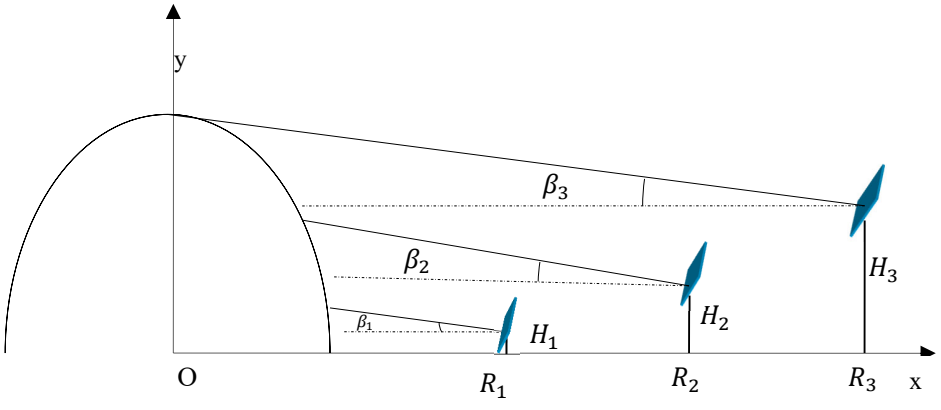

Fig. 2. Heliostat distribution study according to angles $\beta_1, \beta_2, \beta_3$to 2D

2. Discretization of the heat transfer matrix

Among the main elements of desalination is the glass used during this process. Several 10 cm thick glass plates were glued next to each other with 10 cm thick steel bars, to withstand the vibrations caused by the wind and withstand the pressure resulting from the temperature high inside the dome. The outer dome surface area of 2513.3 m² receives a heat $\dot{q}_{\lambda,solar}$ assumed to be uniform over the entire dome surface. The heat transfer model will be described in order to analyze the thermal behavior as a function of different physical parameters below:

-Heat and water exchange by direct injection and withdrawal of water;
-Heat exchange by conduction through the wall of the dome
-Exchanges by natural convection inside the dome.
-The system is in an almost stationary state.
-The transmission α_g' of glass is about 99%
-Room temperature is $T_a = T_{sky} = 298K$
-The thermo-physical properties of water are constant,
-The heat losses to the outside of the tank are unidirectional.
-Condensation occurs only on the cover (there is no condensation on the side walls).
-The mass of the glass and the water are negligible.
-The volume of the hemispherical dome 33,493.33 m^3
-The concentration of the brine is not involved in the heat and mass transfers from and to the brine

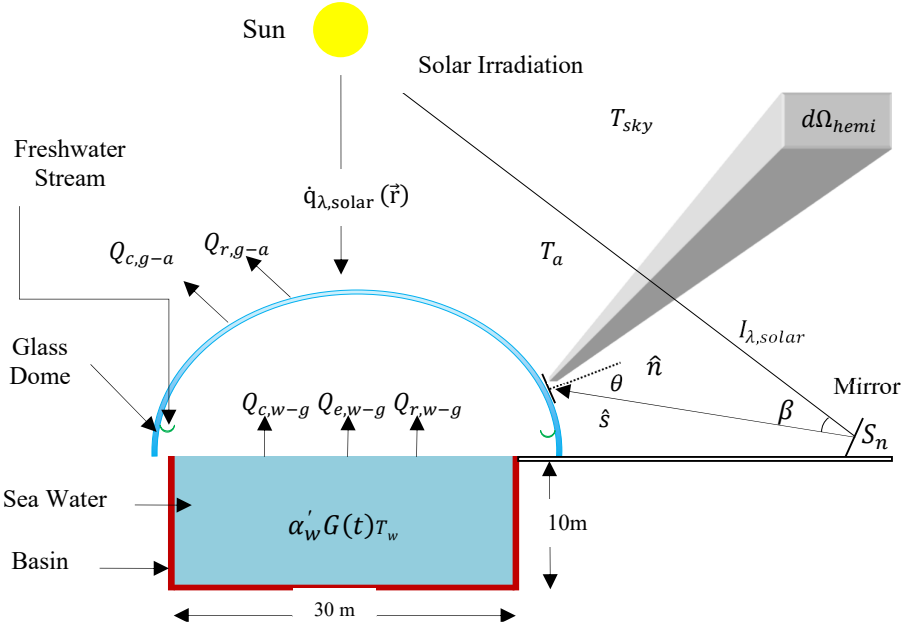

Fig. 3. Representation of heat production process by DNI

The temperature variation of (T_g, T_w) hemispherical dome, dirty water is a manifestation of a set of thermal intervening (see Fig.3) on different(Ashour et al., 2021; Hong et al., 2019) point of the internal surface of the dome.

Table 1. energy balance integrated in water desalination

Energy type	Formula	Developed formula
Conduction energy $Q_{c\,w-g}$	$h_{c\,w-g}(T_w - T_g)$	$h_{c\,w-g} = 0{,}884\sqrt[3]{(T_w - T_g) + \frac{(P_w - P_g)(T_w + 273)}{268{,}9 \times 10^3 - P_w}}$
Vaporization energy $Q_{e\,w-g}$	$h_{e\,w-g}(T_w - T_g)$	$h_{e\,w-g} = (16{,}28 \times 10^{-3}) h_{c\,w-g} \frac{(P_w - P_g)}{(T_w - T_g)}$
Radiation energy $Q_{r\,w-g}$	$h_{r\,w-g}(T_w - T_g)$	$\varepsilon_{eff}\sigma\left[(T_w + 273)^4 + (T_g + 273)^4\right]$
Radiation energy $Q_{r\,g-a}$	$h_{r\,g-a}(T_g - T_{sky})$	$\varepsilon_g\sigma\left[(T_g + 273)^4 + (T_{sky} + 273)^4\right]$
Conduction energy $Q_{c\,g-a}$	$h_{c\,g-a}(T_g - T_a)$	

Table 1 summarizes all of these energies that go into the heat transfer process by describing the types of energies and their characteristic semi-expanded and expanded formulas in order to combine and organize its formulas in an energy balance of the studied system.

Energy balance for the glass dome

$$Q_{c,g-a} + Q_{r,g-a} + m_g c_g \frac{\partial T_g}{\partial t} = \alpha'_g \dot{q}_{\lambda,solar}(\vec{r}) + Q_{c,w-g} + Q_{e,w-g} + Q_{r,w-g} - Q_{c,g-a} - Q_{r,g-a} u \quad (3)$$

$$m_g c_g \frac{\partial T_g}{\partial t} = \alpha'_g G(t) + \left(h_{c,w-g} + h_{r,w-g} + h_{e,w-g}\right)\left(T_w - T_g\right) - h_{r,g-a}\left(T_g - T_{sky}\right) + h_{c,g-a}\left(T_g - T_a\right) \quad (4)$$

$$\frac{\partial T_g}{\partial t} = \frac{\alpha'_g}{m_g c_g} \dot{q}_{\lambda,solar}(\vec{r}) + \alpha_{11} T_w + \alpha_{12} T_g + \alpha_{13} T_{sky} + \alpha_{14} T_a \quad (5)$$

Energy balance for salt water

$$\alpha'_w G(t) + Q_{c,b-w} = Q_{c,w-g} + Q_{e,w-g} + Q_{r,w-g} + m_w c_w \frac{\partial T_w}{\partial t} \quad (6)$$

$$m_w c_w \frac{\partial T_w}{\partial t} = \alpha'_w G(t) + h_{c,b-w}(T_b - T_w) - \left(h_{c,w-g} + h_{r,w-g} + h_{e,w-g}\right)\left(T_w - T_g\right) \quad (7)$$

$$\frac{\partial T_w}{\partial t} = \frac{\alpha'_w}{m_w c_w} G(t) - \alpha_{21} T_w + \alpha_{22} T_g + \alpha_{23} T_b \quad (8)$$

Finally, Eq. (5) to Eq. (8) are arranged and connected with each other to obtain an integrated one, as presented in matrix (9)

$$\frac{\partial}{\partial t}\begin{pmatrix} T_g \\ T_w \end{pmatrix} = \begin{pmatrix} \alpha_{12} & \alpha_{11} & 0 \\ \alpha_{22} & -\alpha_{21} & \alpha_{23} \end{pmatrix} \begin{pmatrix} T_g \\ T_w \\ T_b \end{pmatrix} + \begin{pmatrix} \frac{\alpha'_g}{m_g c_g} \\ \frac{\alpha'_w}{m_w c_w} \end{pmatrix} \left(\dot{q}_{\lambda,solar}(\vec{r})\right) + \begin{pmatrix} \alpha_{13} T_{sky} + \alpha_{14} T_a \\ 0 \end{pmatrix} \quad (9)$$

The matrix (9) describes the temperature variation (T_g, T_w) (as a function of the amount of radiation received at the surface of the solar dome, the sky temperature$T_{sky}$and ambient temperatureT_a. The coefficient α_{ij} sum up all the parameters integrated at the base of the Eqs. (4-6) which will be fulfilled according to the parameter illustrated in Table 2. The study of the evolution of the wall temperature $T_b$of the basin will not be taken into account because the factor of heat exchange by convection between the salt water and the wall and considered higher which allows neglecting the heat losses at the level of the wall. On the other hand, there are many methods (Wang et al., 2021) for the resolution of the matrix (9), like the method of Euler, Taylor, finite difference, but these methods remain long and complex against a matrix in the form of a differential equation of order 4. The efficiency Range Kutta method of order 4 was adopted in the numerical resolution of the system obtained. An implicit and explicit iterative development of the RK4 method is carried on the matrix 9 presented via formula (10).

$$\Gamma(t_{n+1}) = \Gamma(t_n) + hf(t_n, t_n) \quad (10)$$

This temporal discretization presented by Eq. (10) is subsequently be modeled on Matlab with the creation of an implantation while respecting the optical parameters demonstrated previously and the physical parameters shown in Table 2.

Table 2. Optical parameters for water

Parameters	Liquid water	Air
Volumic mass	998 ,20Kg/m^3	1,2250 Kg/m^3
Thermal conductivity	0,6000W/m, ℃	0,024200W/m, ℃
Specific heat	4182,0 J/Kg, ℃	1006,4J/Kg, ℃
Viscosity	0,00130Pa-s	1,7849e^{-5}Pa − s
Latent Heat	2,2631e^{+6} J/Kg	
Vaporization temperature	10,850℃	
Formation Entropy	69902J/℃	

2.1 Pressure and humidity rate

After having determined the temperature difference between the glass and the dirty water, it is necessary to determine the quantity of water evaporated in the solar dome and the dew temperature (Lv et al., 2021) which will be presented as a function of the humidity and the temperature saturated water. However, there are many mathematical formulas making it possible to estimate the rate of evaporation according to the temperature and the pressure of the water, like the approximate equation of Goff - Gratch and Magnus – Tetens (Wan et al., 2018), but this remains complex and requires many parameters. However, the Jordan Buck equation is characterized by precision and easy application. This equation describes the evolution of the saturated vapor pressure of water vapor as a function of the air temperature inside the solar dome, which can be written in two different forms, as is the case in Eq. (11).

$$P_{ws}(T) = ae^{\left(b-\frac{T}{234,5}\right)\left(\frac{T}{c+T}\right)} \tag{11}$$

The values of a, b, c are parameters as a function of the air temperature and the saturated vapor pressure in mbar, are given according to Arden Buck (Pakari & Ghani, 2019) .

a = 6.1121 mbar, b = 17.368, c = 238.88 °C; for 0 °C ≤ T ≤ 50 °C (error ≤ 0.05%).

a = 6.1121 mbar, b = 17.966, c = 247.15 °C; for −40 °C ≤ T ≤ 0 °C (error ≤ 0.06%).

In addition, Eq. (11) leads to the determination of the humidity level of the indoor air calculated as a function of the water vapor in the air of the dome. It varies from $0gm^3$ in dry air to $30gm^3$ when the vapor is saturated till 30℃. It can reach 100% relative humidity when the partial pressure of water vapor P_w is equal to the saturated vapor pressure. The humidity in our case will be given by the formula (12).

$$\begin{cases} \phi = \dfrac{P_w}{P_{ws}} \\ \phi = 100\% \text{ donc } P_w = P_{ws} = ae^{\left(b-\frac{T}{234,5}\right)\left(\frac{T}{c+T}\right)} \end{cases} \tag{12}$$

The condensation of the hot water inside the glass dome and the study of the percentage of vapor which was expressed as a function of the humidity coefficient led to the measurement of the dew temperature formed on the glass cover and it is given by formula (13).

$$T_{dp} = \frac{c \ln \frac{\phi \times e^{\left(b-\frac{T}{234,5}\right)\left(\frac{T}{c+T}\right)}}{100}}{b - \ln \frac{\phi \times e^{\left(b-\frac{T}{234,5}\right)\left(\frac{T}{c+T}\right)}}{100}} \tag{13}$$

Eq. (12) calculates the temperature (T_{dp}) as a function of the relative humidity (ϕ) and the air temperature inside the solar dome. On the other hand, the pressure of dirty water and glass cannot be neglected due to its interference in the depth of the energy transformation process. For this, we program algorithms on Matlab in order to determine the pressure evolution of the two components using Eq. (14) illustrated in reference (Wojtasik et al., 2020) by using the parameters of Table 2.

$$\begin{cases} P_g = e^{25{,}273-\frac{5144}{Tg+273}} \\ P_w = e^{25{,}273-\frac{5144}{T_w+273}} \end{cases} \quad (14)$$

2.2. Quantity of water produced

The amount of H_2Owhich can occur at the internal glass level after condensation will be linked to the saturation pressure and the dew temperature and also the total volume of the solar dome. This quantity will be estimated by the law of perfect gaz.

$$m_{H_2O} = M(H_2O)\frac{\mathrm{P_{ws}}}{\mathrm{R} \times T_{dp}} \quad (15)$$

3. Results and discussions

The mathematical description makes it possible to develop an algorithm on Matlab to validate the test carried out on all the equations found during this study. Fig. 4 presents the results of the modelling of Eq. (1) on the basis of the metrological conditions of the Moroccan region of Rabat–Salé-Kénitra, which has geographic coordinates, Latitude: 34.0242, Longitude: -6.8227 34 ° 1 ′ 27 ″ North, 6° 49 ′ 22 ″ West, and also by considering the parameter β the angle of inclination of the heliostats which varies between 0° and 90°. Regarding the two angles θ and φ, they will not interfere in the calculation of the amount of solar radiation in a direct way, but they will be taken into account in the calculation of the concentration rate as shown in Eq. (2). In this case $\theta$and φwill be varied over two different interval;$\theta = [0{,}90°]$and $\varphi = [0{,}360°]$.

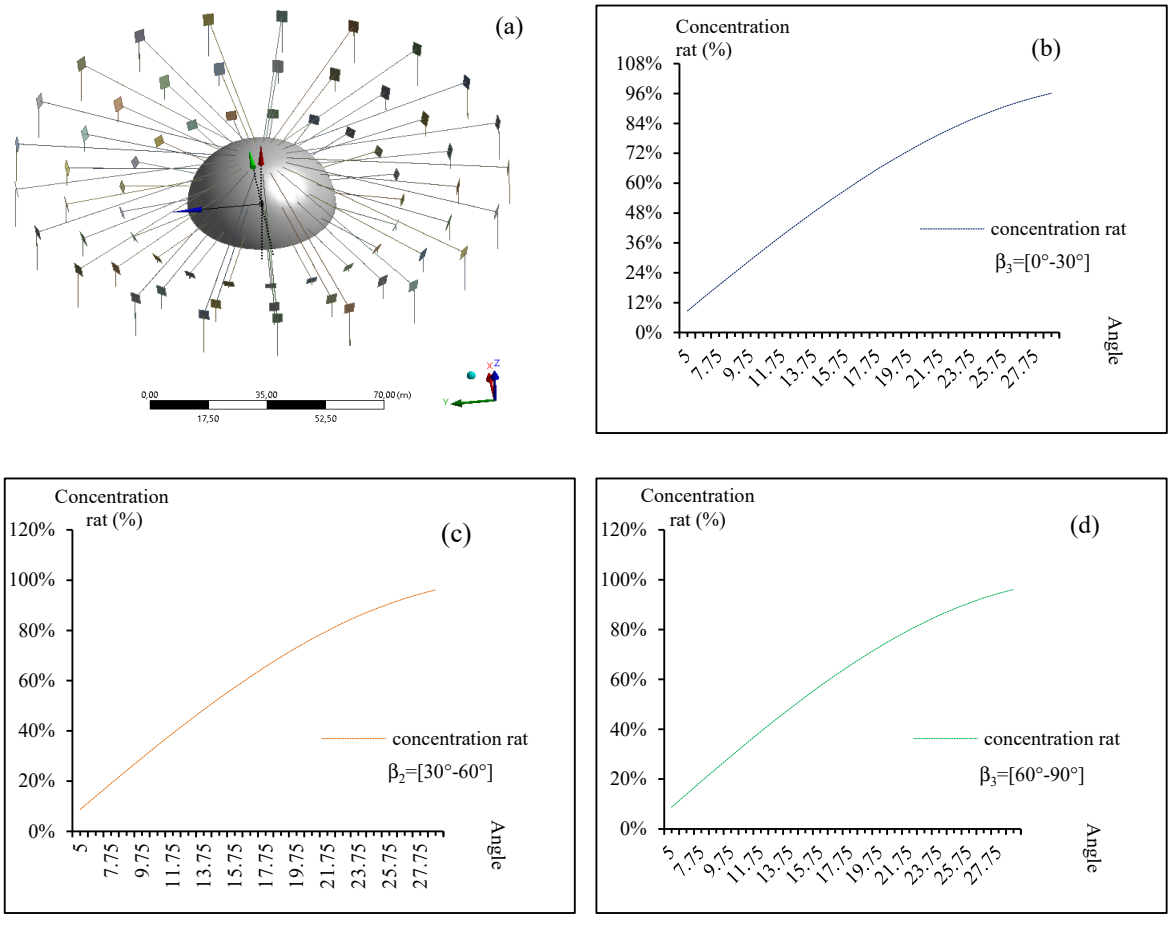

Fig.4. Solar ray concentration depending on the angle $\beta_1 = [0-30°], \beta_2 = [30-60°], \beta_3 = [60-90°]$.

Fig. 5 presents the results obtained by the DNI calculated via Matlab in the form of a concave curve. This curve is

compared with the results of PVGIS during the same day respecting the parameters indicated in Table 2. This comparison shows the change which took place in the solar radiation reflected on the solar dome. Since sunrise, an accelerated increase in flow was recorded until noon. After that, the simulated DNI experienced a sudden change when reaching the maximum value of 1080w / m² for two hours, despite the continuous increase in solar flux from PVGIS. It is noted that this problem is also known by the solar tower system (Ghirardi et al., 2021), which has been confirmed by the experimental measurements mentioned in references (Ashour et al., 2021; Li et al., 2019; Marugán-Cruz et al., 2020). This is explained by the fact that the incineration angle β reaches its maximum in the interval $[0-70°]$ and not in the interval $[0-90°]$as indicated above by the concentration rate shown in Fig.5 (b). In Fig.6, we notice that there is an increase in the concentration rate by comparing with the experimental measurements illustrated by the reference (Mahmoud et al., 2019), up to a maximum value of 78% of concentration when the angle βclose 90°. To correct this low concentration we separated the angle βover three intervals $\beta_1 = [0-30°], \beta_2 = [30-60°], \beta_3 = [60-90°]$ then redone the calculation on Matlab based on a 3D geometric shape obtained by the Ansys software (see Fig.4 (a).

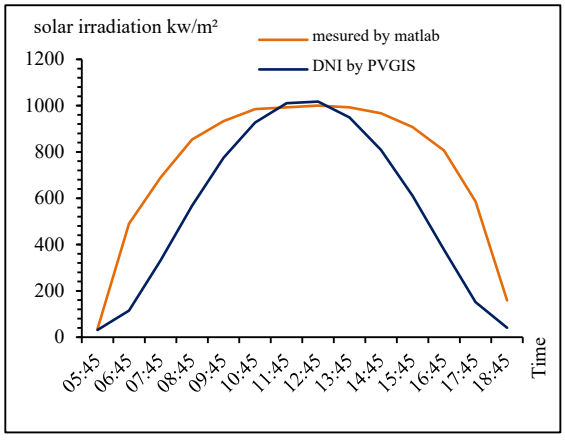

Fig.5.DNI simulation by Matlab

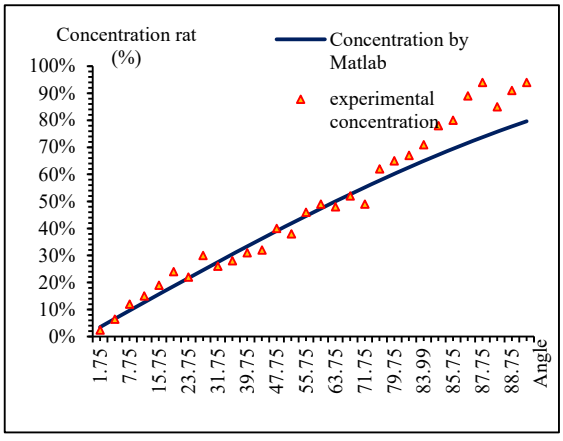

Fig.6. Solar ray concentration depending on the angle$\beta = [0-90°]$.

In Fig.4(a), one notices the distribution of solar radiation in 3D on the hemispherical dome with an azimuth angle of $\varphi = 360°$and height angleθ varies from$0°$to$90°$. This distribution obtained according to geometric block functions constructed with parameters from Table 2. On the other hand, this distribution makes it possible to have a higher concentration rate and close to 100% for each part (see Fig.4 (b-c-d) which was not feasible for the first test. This result is explained by the fact that the solid angle of solar dome $d\Omega_{dome}$completely coincides with the solid angle $d\Omega_h$of each heliostat in the solar dome power plant while contributing to a reflection of 99% of solar radiation which increases the glass temperature hemispherical and also the dirty water temperature. In conclusion, these results confirm that it may be useful to use motors (Shylaja et al., 2021) which help track the sun's rays during the day falling on the shape of the dome to reduce energy consumption.

3.1 Temperature of glass and salt water

The separation of the angles of inclination β led to a review of the matrix resolution method (9), especially for the solar dome glass temperatureT_g. The mesh technique has been included to enhance the results because this part is the main element in the heat transfer mentioned above (see Table 1). The dome was divided into 10,000 area units of 0.1 m². The results obtained are illustrated in Fig. 7.

Fig.7 illustrates the variation in glass temperature as a function of the inclination angle β. The meshing function on Matlab (Smitha and Nagaraja 2019; Sonker et al., 2019) allows comparing the distributionT_g over each 0.1 m² of hemispherical dome area. Based on Fig. 7(b) a uniform distribution of the temperature is seen for the angles $\beta_1, \beta_2, \beta_3$against a weak distribution of $T_g$illustrated on the Fig.7 (a), which predicts a significant rise in the temperature of the glass as well as the pressure. The results obtained assure the importance of the inclination angle separation and its impact on the construction of the solar dome plant.

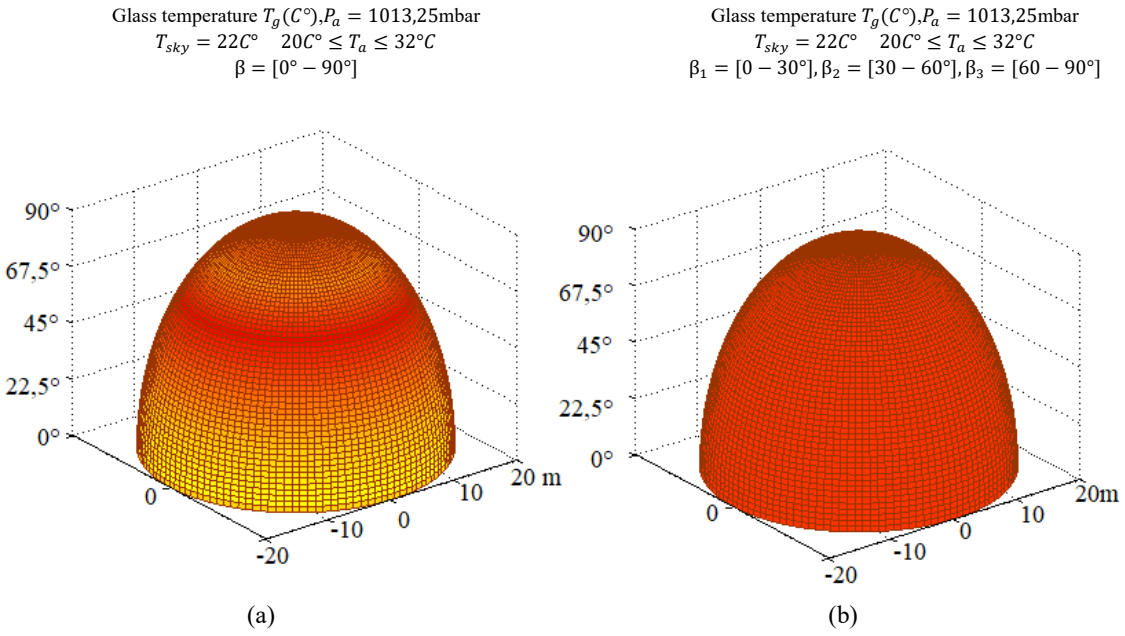

Fig. 7. Glass temperature $T_g(C°)$ as a function of the angle of inclination.

3.2 Validation of heat transfer matrix by RK4 on Matlab

The execution of the numerical algorithms carried out to solve the matrix 9 led to obtain results illustrated in Fig.8 and 9 and 10. These results are verified using the experimental studies cited in reference (Gil et al., 2021) .

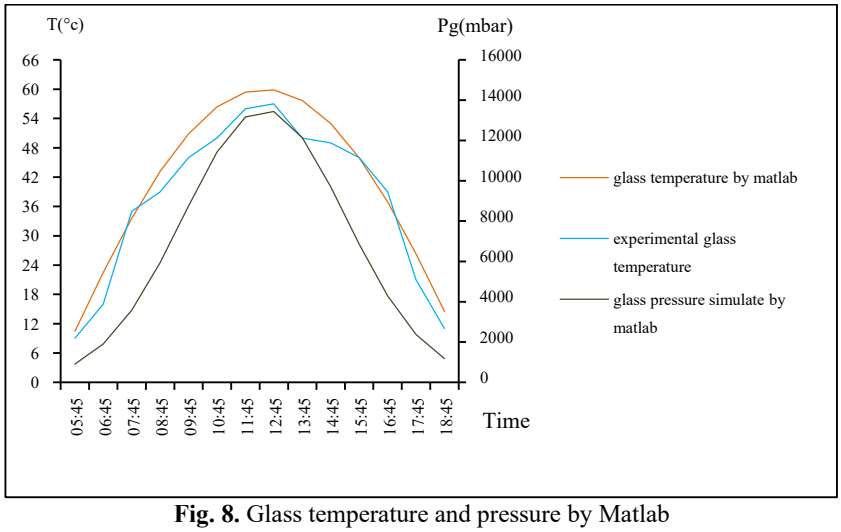

Fig. 8. Glass temperature and pressure by Matlab

Fig. 8 represents the variation in the temperature of glass used under metrological conditions in the Rabat-Salé-Kenitra region, with an initial pressure P_a1013,25 mbar and $T_{sky} = 22C°$ $20C° \leq T_a \leq 32°C$. These measurements are taken for every 0.1 m² of sun dome area. On the other hand, a significant increase in the temperature of the glass used was recorded, comparing with experimental measurements (Guo et al., 2020) during the morning. The temperature of the glass increases until it reaches a maximum value of 70°C at noon and then begins to decrease. This decrease is due to the change of position of the sun relative to the earth; result well explained previously by the change of the angle of inclination β on the three intervals of angles. Despite this variation, the glass temperature distribution $T_g$with respect to the angles $\theta = [0° - 90°]$and $\varphi = [0° - 360°]$ remains uniform throughout the day, which ensures the presence of internal heat throughout the day. This result is consistent with the results obtained previously in Fig.7 (a-b). The pressure was also calculated by an algorithm developed based on equation (14) while respecting the parameters of the glass used. We notice that there is a significant increase in temperature during the same period, then it begins to decrease after reaching a maximum value of $1{,}4 \times e^4 mbar$. The high pressure produced is considered to be one of the main factors that directly interfere in the desalination process, such

as condensation, evaporation and the production of fresh water.

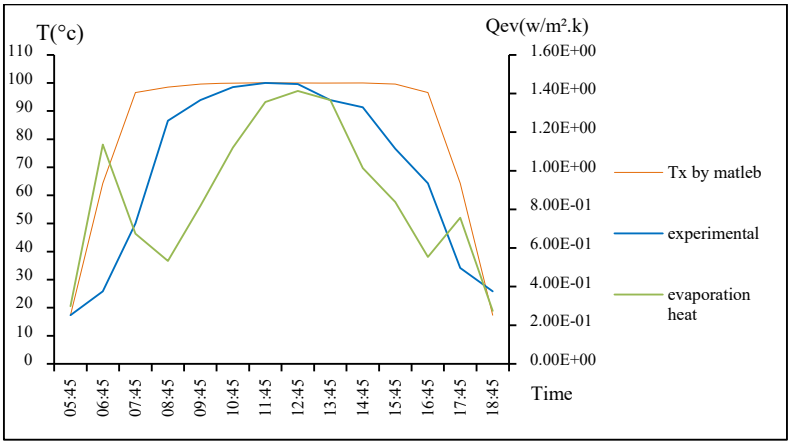

Fig. 9. Temperature of water basin and evaporative energy

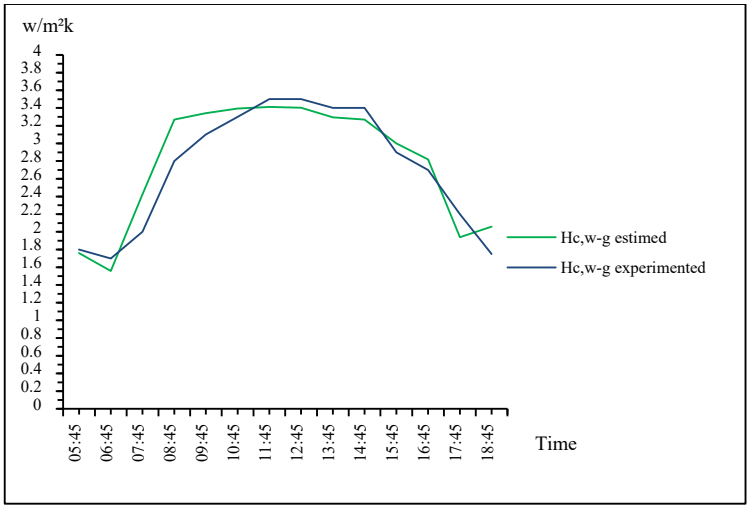

Fig.10. Convective heat transfer coefficient from water to glass cover with respect to time

Fig. 9 shows the results obtained concerning the evolution of the water temperature $T_w$in the basin. It is noted that the temperature obtained is only related to the surface of the basin and not to its depth. Comparing with(Hong, Wang, and Park 2019) , these measurements indicate a significant increase in the temperature of the water until it reaches the maximum value of 100°c under pressure 1019.25 mbar where the evaporation process begins on a period of 4 to 6 hours. Evaporative energy was disturbed early in the morning due to the parameter of fluctuating pressure of saturation of water molecules after it continued to increase significantly. Fig.10 illustrates the variation of the heat exchange coefficient between water and glass by comparing with experimental results cited in references 1 and 2. The results indicate a positive increase in the heat exchange coefficient until reaching a maximum of 3.5 w / m²k confirmed by the evaporation energy curve.

Fig. 11 presents the simulation results obtained thanks to the algorithms formulated on Matlab, which relate to each of the changes in temperature of the dew point, which have been compared with the experimental results in references(Ghirardi et al., 2021; Hong, Wang, and Park 2019) on each 0.1m². It can be noticed that there is a marked change in the temperature of the water points without exceeding the ratio of 53 degrees, which corresponds to the initial conditions which were previously approved. The percentage of pressure saturated with water inside the dome is improved, because we notice the increase in pressure proportional to the dew temperature, which exceeds the value of 8000, which positively influences the humidity rate, as shown in Fig.12. Where we notice that the humidity increases rapidly, especially in the evening, which indicates a decrease in the concentration of rays at their levels, which indicates a decrease in the temperature of the glass and the beginning of the production process of fresh water where one clearly notices the increase in the percentage of water, especially if one compares the experimental values together (Jahanpanah et al., 2021; Kumar et al.2020; Modi et al., 2019).

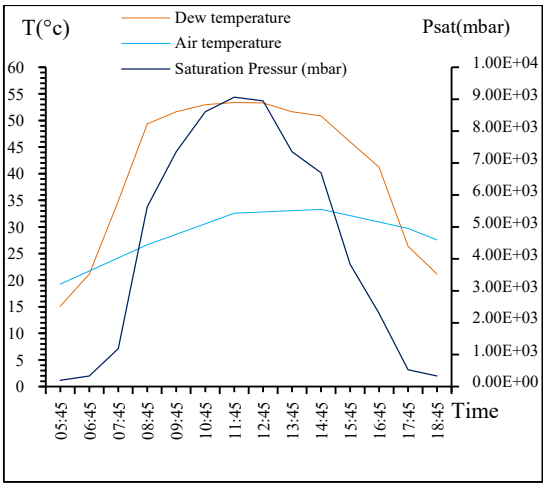

Fig.11. Dew point temperature and saturation pressure

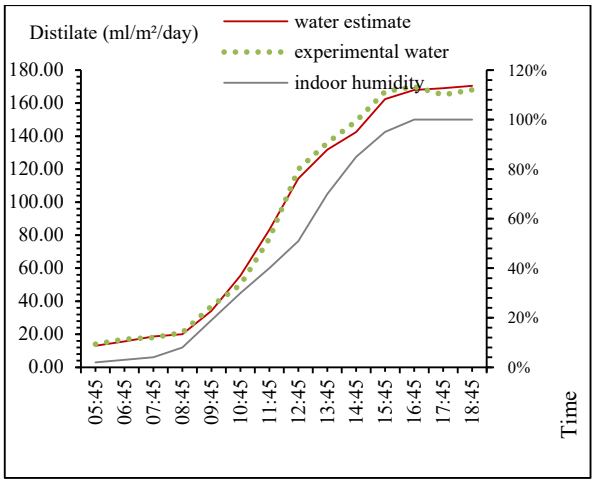

Fig.12. Fresh water production

4. Conclusion

In this article, the solar dome technology has been highlighted in order to present its features and advantages. A geometric and optical study was carried out using Matlab and Ansys software. The amount of radiation that can produce using 60 heliostats has been verified and analysed according to the tilt angle study. The results obtained showed that fixing the angle of inclination in angular intervals achieves a 99% concentration rate resulting in an improvement in the amount of radiation received by the hemispherical dome. The analyses are also carried out on the temperature of glass and dirty water. The results mean that the dome can reach temperatures between 60 ° C and 70 ° C without impacting by the pressure. The amount of evaporation produced increases the humidity level which increases the saturation pressure to produce fresh water. Finally, solar dome technology can be an effective solution to deal with most of the problems that arise in other technologies such as rust in thermal evaporators and the high costs of reverse osmosis technology. On the other hand, the results achieved offer a precious opportunity to countries which have a high solar flow throughout the year, such as Morocco.

Acknowledgments

This work is supported by the team renewable energy of Ibn-Tofail university Kenitra ,Morocco.

References

Ali, E. S., Mohammed, R. H., Qasem, N. A., Zubair, S. M., & Askalany, A. (2021). Solar-powered ejector-based adsorption desalination system integrated with a humidification-dehumidification system. *Energy Conversion and Management*, *238*, 114113.

Anand, B., Shankar, R., Murugavelh, S., Rivera, W., Prasad, K. M., & Nagarajan, R. (2021). A review on solar photovoltaic thermal integrated desalination technologies. *Renewable and Sustainable Energy Reviews*, *141*, 110787.

Ashour, A. I., Almitani, K. H., & Abu-Hamdeh, N. H. (2021). Developing and improving a prototype scale concentrating solar power tower-system. *Sustainable Energy Technologies and Assessments*, *45*, 101105.

Bekker, A., Van Dijk, M., Niebuhr, C. M., & Hansen, C. (2021). Framework development for the evaluation of conduit hydropower within water distribution systems: A South African case study. *Journal of Cleaner Production*, *283*, 125326.

Bonanos, A. M., Faka, M., Abate, D., Hermon, S., & Blanco, M. J. (2019). Heliostat surface shape characterization for accurate flux prediction. *Renewable energy*, *142*, 30-40.

Chauhan, V. K., Shukla, S. K., Tirkey, J. V., & Rathore, P. K. S. (2021). A comprehensive review of direct solar desalination techniques and its advancements. *Journal of Cleaner Production*, *284*, 124719.

ElHelw, M., El-Maghlany, W. M., & El-Ashmawy, W. M. (2020). Novel sea water desalination unit utilizing solar energy heating system. *Alexandria Engineering Journal*, *59*(2), 915-924.

Figueroa, A., Jackiewicz, Z., & Löhner, R. (2021). Efficient two-step Runge-Kutta methods for fluid dynamics simulations. *Applied Numerical Mathematics*, *159*, 1-20.

Ghirardi, E., Brumana, G., Franchini, G., & Perdichizzi, A. (2021). Heliostat layout optimization for load-following solar tower plants. *Renewable Energy*, *168*, 393-405.

Gil, B., Fievez, A., & Zajaczkowski, B. (2021). Pool boiling heat transfer coefficient of dimethyl ether and its azeotropic ternary mixtures. *International Journal of Heat and Mass Transfer*, *171*, 121063.

Guo, R. F., Zhang, L., Mo, D. M., Wu, C. M., & Li, Y. R. (2020). Measurement of temperature profile near the evaporating

interface in an annular pool with radial temperature gradients at low pressures. *Experimental Thermal and Fluid Science*, *119*, 110221.

Hong, S. J., Wang, E. S., & Park, C. W. (2019). Heat transfer characteristics of falling film and pool boiling evaporation in hybrid evaporator in vapor compression system. *Applied Thermal Engineering*, *153*, 426-432.

Jahanpanah, M., Sadatinejad, S. J., Kasaeian, A., Jahangir, M. H., & Sarrafha, H. (2021). Experimental investigation of the effects of low-temperature phase change material on single-slope solar still. *Desalination*, *499*, 114799.

Mohamed, A. M. O., Paleologos, E. K., & Howari, F. (Eds.). (2020). *Pollution Assessment for Sustainable Practices in Applied Sciences and Engineering*. Butterworth-Heinemann.

Khlaifat, A., Batarseh, M., Nawayseh, K., Amira, J., & Talafeha, E. (2020). Mixing of Dead Sea and Red Sea waters and changes in their physical properties. *Heliyon*, *6*(11), e05444.

Kumar, D., Layek, A., & Kumar, A. (2020, November). Performance enhancement of single slope solar still integrated with flat plate collector for different basin water depth. In *AIP Conference Proceedings* (Vol. 2273, No. 1, p. 050007). AIP Publishing LLC.

Lai, X., Long, R., Liu, Z., & Liu, W. (2021). Solar energy powered high-recovery reverse osmosis for synchronous seawater desalination and energy storage. *Energy Conversion and Management*, *228*, 113665.

Li, X., Wang, Z., Yang, M., & Yuan, G. (2019). Modeling and simulation of a novel combined heat and power system with absorption heat pump based on solar thermal power tower plant. *Energy*, *186*, 115842.

Lin, S., Zhao, H., Zhu, L., He, T., Chen, S., Gao, C., & Zhang, L. (2021). Seawater desalination technology and engineering in China: A review. *Desalination*, *498*, 114728.

Liu, S., Wang, Z., Han, M., & Zhang, J. (2021). Embodied water consumption between typical desalination projects: Reverse osmosis versus low-temperature multi-effect distillation. *Journal of Cleaner Production*, *295*, 126340.

Lrhoul, H., El Assaoui, N., & Turki, H. (2021). Mapping of water research in Morocco: A scientometric analysis. *Materials Today: Proceedings*, *45*, 7321-7328.

Lv, J., Xu, H., Xu, T., Liu, H., & Qin, J. (2021). Study on the performance of a unit dew-point evaporative cooler with fibrous membrane and its application in typical regions. *Case Studies in Thermal Engineering*, *24*, 100881.

Mahmoud, A., Fath, H., Ookwara, S., & Ahmed, M. (2019). Influence of partial solar energy storage and solar concentration ratio on the productivity of integrated solar still/humidification-dehumidification desalination systems. *Desalination*, *467*, 29-42.

Marugán-Cruz, C., Sánchez-Delgado, S., Gómez-Hernández, J., & Santana, D. (2020). Towards zero water consumption in solar tower power plants. *Applied Thermal Engineering*, *178*, 115505.

Modi, K. V., Shukla, D. L., & Ankoliya, D. B. (2019). A comparative performance study of double basin single slope solar still with and without using nanoparticles. *Journal of Solar Energy Engineering*, *141*(3), 031008.

Mwandila, G., Mwanza, M., Sikhwivhilu, K., Siame, J., Mutanga, S. S., & Simposya, A. (2021). Modeling energy requirements for a biogas-supported decentralized Water treatment systems for communities in chambishi (Zambia) and diepsloot (South Africa) townships. *Renewable Energy Focus*, *37*, 20-26.

Nyiwul, L. (2021). Climate change adaptation and inequality in Africa: Case of water, energy and food insecurity. *Journal of Cleaner Production*, *278*, 123393.

Ouda, M., Kadadou, D., Swaidan, B., Al-Othman, A., Al-Asheh, S., Banat, F., & Hasan, S. W. (2021). Emerging contaminants in the water bodies of the Middle East and North Africa (MENA): A critical review. *Science of the Total Environment*, *754*, 142177.

Pakari, A., & Ghani, S. (2019). Comparison of 1D and 3D heat and mass transfer models of a counter flow dew point evaporative cooling system: Numerical and experimental study. *International Journal of Refrigeration*, *99*, 114-125.

Patel, S. K., Singh, D., Devnani, G. L., Sinha, S., & Singh, D. (2021). Potable water production via desalination technique using solar still integrated with partial cooling coil condenser. *Sustainable Energy Technologies and Assessments*, *43*, 100927.

Shukla, S. K. (2021). Use of Quantum Dots Polymer and its Composite for Water Purification Through Solar Desalination.

Shylaja, G., Venkatesh, B., Naidu, V. K., & Murali, K. (2021). Two-dimensional non-uniform mesh generation for finite element models using MATLAB. *Materials Today: Proceedings*, *46*, 3037-3043.

Smitha, T. V., & Nagaraja, K. V. (2019). Application of automated cubic-order mesh generation for efficient energy transfer using parabolic arcs for microwave problems. *Energy*, *168*, 1104-1118.

Sonker, V. K., Chakraborty, J. P., Sarkar, A., & Singh, R. K. (2019). Solar distillation using three different phase change materials stored in a copper cylinder. *Energy Reports*, *5*, 1532-1542.

Vega-Rodriguez, M. A., Perez, C. J., Reder, K., & Floerke, M. (2021). A stage-based approach to allocating water quality monitoring stations based on the WorldQual model: The Jubba River as a case study. *Science of The Total Environment*, *762*, 144162.

Wan, Y., Lin, J., Chua, K. J., & Ren, C. (2018). A new method for prediction and analysis of heat and mass transfer in the counter-flow dew point evaporative cooler under diverse climatic, operating and geometric conditions. *International Journal of Heat and Mass Transfer*, *127*, 1147-1160.

Wang, Z., Zheng, X., Chryssostomidis, C., & Karniadakis, G. E. (2021). A phase-field method for boiling heat transfer. *Journal of Computational Physics*, *435*, 110239.

Wojtasik, K., Rullière, R., Krolicki, Z., Zajaczkowski, B., & Bonjour, J. (2020). Subcooled boiling regime map for water at

low saturation temperature and subatmospheric pressure. *Experimental Thermal and Fluid Science*, *118*, 110150.
Xiao, G., Zeng, J., & Nie, J. (2021). A practical method to evaluate the thermal efficiency of solar molten salt receivers. *Applied Thermal Engineering*, *190*, 116787.